Control of Isolated Differential-Mode Single- and Three-Phase Ćuk Inverters at Module Level

Harshit Soni, Sudip K. Mazumder, *Fellow, IEEE*, Ankit Gupta, *Student Member, IEEE*, Debanjan Chatterjee, and Abhijit Kulkarni, *Member, IEEE*

***Abstract*—In this paper, a modular control approach has been proposed for a single- and three-phase differential-mode Ćuk inverter (DMCI) operating with a recently proposed discontinuous-modulation scheme that offers tangible performance benefits over conventional continuous modulation scheme. The modular control scheme uses a combination of a transformation and adaptive control law to meet tracking requirements in the presence of converter nonlinearity. Experimental results for the single- and three-phase DMCI are provided for startup, steady state, load transition, and total harmonic distortion using different types of loads, which validate the efficacy of the implemented modular tracking controller. Further, detailed stability of the closed-loop DMCI module is provided.**

***Index Terms*—Adaptive control, differential-mode Ćuk inverter (DMCI), high-frequency link (HFL), single- and three-phase, moduation, stability.**

I. Introduction

HIGH-FREQUENCY-LINK (HFL) inverters have been described in details in the literature [1]–[4]. A compact class of HFL inverters—differential-mode Ćuk inverter (DMCI) (see Fig. 1)—with plurality of advantages, including modularity, scalability, reduced device count, step-up/-down capability, continuous input and output currents, has been operationally demonstrated for multiphase configurations using conventional continuous- and recent discontinuous-modulation schemes (i.e., CMS and DMS) [5]–[9]. DMS-based approach leads to higher energy-conversion efficiency, reduced circulating current, and topological-order reduction. However, DMS-based methodology introduces added nonlinearities due to topological switching. This, unlike CMS-based control approaches [7], [10]–[12] and those based on internal model principle [13], has been addressed using harmonic-compensation-based control [7] and harmonic-compensation and static-feedback-linearization-based control [8]. Both of these control schemes are nonmodular and hence rely on information from more than one module. However, for modular control, a different approach is needed. An outline of this modular-control approach for DMS-based scheme is the focus of this paper. In [9], an initial sketchy outline has been provided in this regard; however, this paper provides details on operating modes, stability proof, control tuning, and additional experimental results.

Unlike the nonmodular control, for the proposed modular control, reference signal for each module is time varying and discontinuous in nature. The controller has a start-up condition at the beginning of each line cycle. Also, for multiphase implementation, the nonlinear loading effect is seen at the module's output terminal. This requires a fast and stable controller which ensures proper tracking. An adaptive control [14] is used to overcome these issues and has been demonstrated experimentally for inverter operation feasibility.

II. DMS Approach for Multiphase DMCI

In DMS-based single-phase DMCI, only one module is activated in negative or positive halves of a line cycle. As such, and as evident in the following equation, the dc voltage-gain relation of the single-phase DMCI is dependent on duty ratios D_1 or D_2

$$\frac{V_{\rm out}}{n\times V_{\rm DC}}=\left(\frac{D_1}{1-D_1}\right),\quad (\text{for}\quad V_{\rm out}>0) \tag{1a}$$

$$\frac{V_{\rm out}}{n\times V_{\rm DC}}=\left(\frac{D_2}{1-D_2}\right),\quad (\text{for}\quad V_{\rm out}<0). \tag{1b}$$

Fig. 2 shows the modes of operation of the DMS-based single-phase DMCI while the modulating signal is captured in Fig. 3. In Figs. 4 and 5, operating modes of the DMS-based three-phase DMCI and the modulating signals are provided.

Unlike the single-phase DMCI, for the three-phase DMCI, operating using DMS, at any given moment, two of the three modules are active. Hence, the dc voltage-gain relation of the three-phase DMCI is described as follows:

$$\frac{V_{{\rm out}ij}}{n\times V_{\rm DC}}=\left(\frac{D_i}{1-D_i}\right)-\delta\left(\frac{D_j}{1-D_j}\right) \tag{2}$$

where i or $j=1,\ 2,\ 3$ and $\delta=1$ if Modules i and j are operating under high-frequency condition while $\delta=0$ if Modules i is operating under high-frequency condition but Module j is not.

Manuscript received August 5, 2017; revised October 13, 2017; accepted November 13, 2017. Date of publication December 4, 2017; date of current version July 15, 2018. This work was supported in part by the U.S. National Science Foundation under Award 1239118. Recommended for publication by Associate Editor S. Kapat. *(Corresponding author: Sudip K. Mazumder.)*

H. Soni is with Tagore Technology, Arlington Heights, IL 60004 USA (e-mail: harshit.blr@gmail.com).

S. K. Mazumder, A. Gupta, and D. Chatterjee are with the Department of Electrical and Computer Engineering, University of Illinois at Chicago, Chicago, IL 60607 USA (e-mail: mazumder@uic.edu; agupta70@uic.edu; dchatt4@uic.edu).

A. Kulkarni is with the Honeywell Technology Solutions Lab. Pvt. Ltd., Bengaluru 560103, India (e-mail: abhiekulkarni@outlook.com).

Color versions of one or more of the figures in this paper are available online at http://ieeexplore.ieee.org.

Digital Object Identifier 10.1109/TPEL.2017.2779408

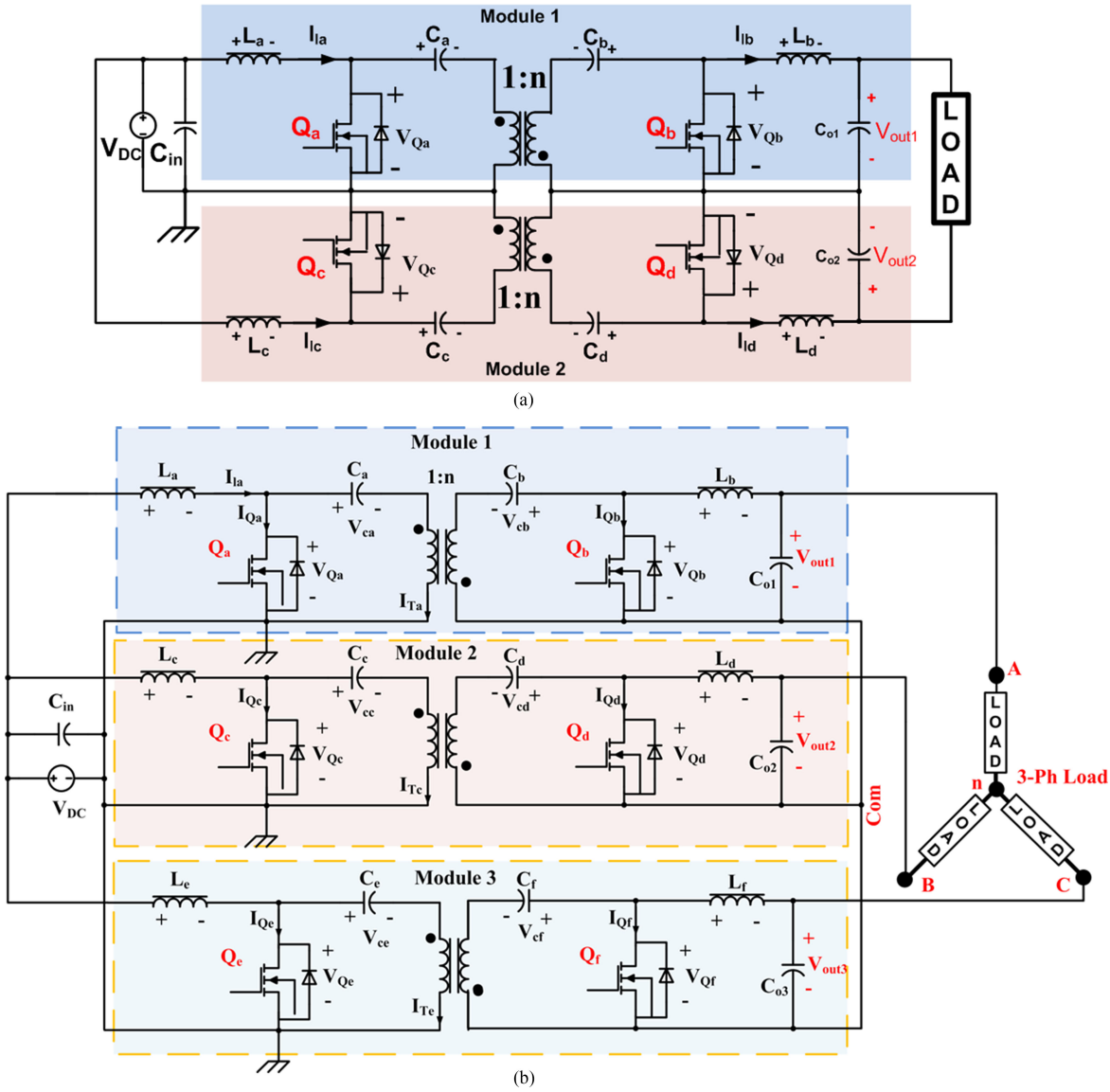

Fig. 1. (a) Single- and (b) three-phase DMCIs. Symbol n represents turns ratio.

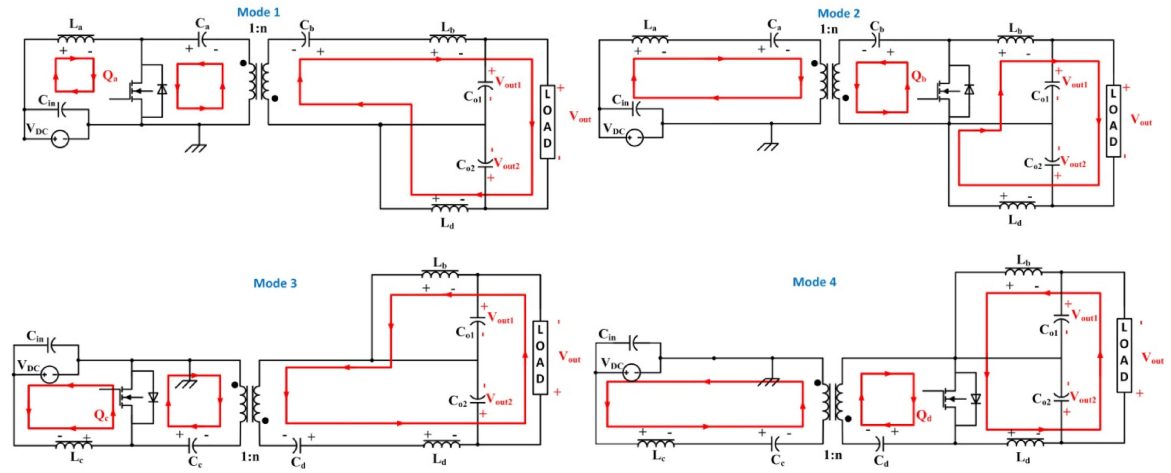

Fig. 2. Operating modes of the single-phase DMCI. Modes 1 and 2 are for positive half of the line cycle while Modes 3 and 4 are for the negative half of the line cycle. For each of the modes, a section of the inverter which is inactive is not shown.

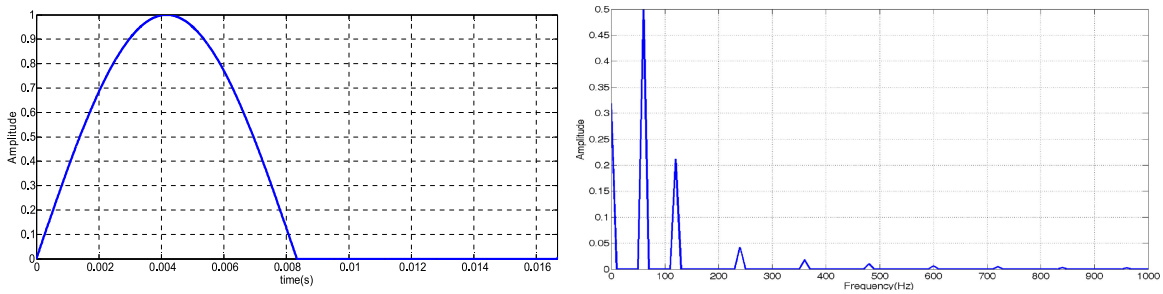

(a) (b)

Fig. 3. (a) Modulating reference signal of one module and its harmonic contents and (b) for the DMS-based single-phase DMCI.

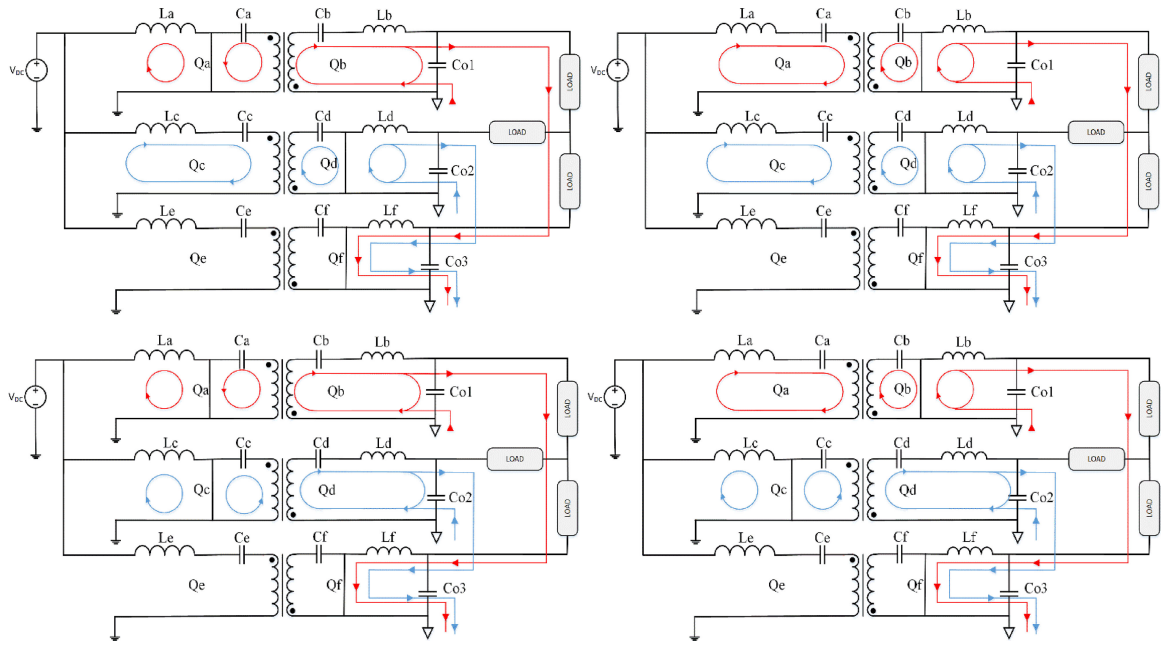

Fig. 4. Operating modes (Modes 1–4) of the three-phase DMCI in particular configuration have been delineated in (a)–(d).

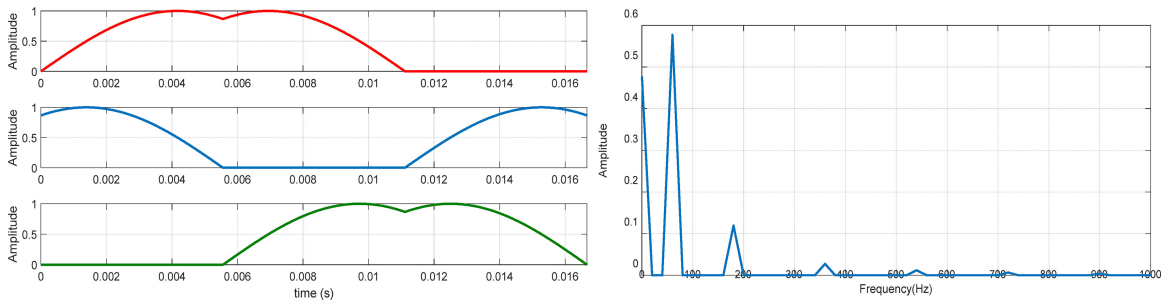

Fig. 5. (a) Modulating reference signals of the three modules of the DMS-based three-phase DMCI and (b) harmonic contents of one of the modulating signals.

III. Modular Control of DMCI

Fig. 6 illustrates the DMS-based modular closed-loop control of a DMCI. A module for the single- or three-phase DMCI is represented as Module x, where x represents the two or three modules (i.e., Modules 1 and 2 or Modules 1 through 3). Because the control of the DMCI is carried out modularly, the outlined control mechanism is illustrated only for one module in Fig. 6. The load is connected to the output of each module. The other end of the load is connected to the other module(s) (for a single- or a three-phase DMCI). The feedback is taken from the output of each module, as shown in Fig. 6. The reference signal (illustrated in Figs. 3 and 5 for single- and three-phase DMCI) of any module is compared to its output voltage and the error voltage is generated. This error voltage is then fed to the

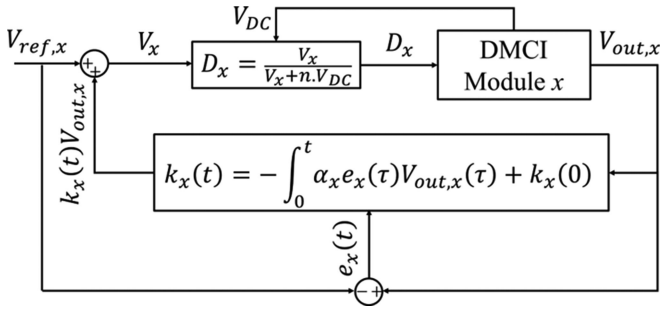

Fig. 6. Illustration of modular control for the single- or three-phase DMCI is provided.

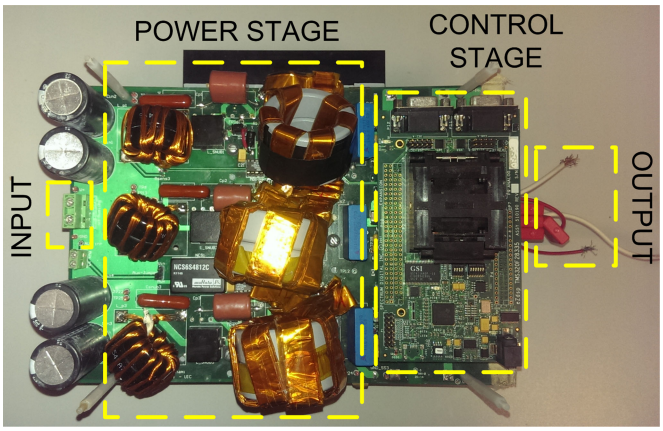

Fig. 7. Experimental multiphase DMCI with the DSP controller.

control block which generates the duty cycle for that module. The switches of each module are modulated based on the duty cycle leading to the synthesis of the desired output voltage.

To implement the modular control scheme, an adaptive control scheme [14] has been adopted which yields fast and stable response for tracking the desired reference output voltage of the module. The adaptive control scheme was developed on the basis of Lyapunov control theory [15], [16], which generates the feedback gain $k_x(t)$ and ensures the stability of the module output voltage. It is found to be the following [17, Sec. III-A]:

$$k_x(t) = -\int_0^t \alpha_x e_x(\tau) V_{\text{out},x}(\tau) + k_x(0) \tag{3}$$

and α_x is the convergence factor which deter how fast the DMCI will stabilize or how rapidly the module output voltage reach the steady state.

The static linearizing block (that converts V_x to D_x using $D_x = V_x/(V_x + nV_{\text{DC}})$ is used here to overcome the nonlinearity between the control input and output voltage of the DMCI [8]. This feedback-gain $k_x(t)$ determination using (3) yields an adaptive system leading to proper tracking along with stability without knowing module parameters. When α_x is large, $k_x(t)$ rapidly converges to a desired equilibrium. The tuning of α_x is carried out experimentally.

The overall control law ensures that the output voltage of DMCI module is stable and tracks the reference voltage closely. If the DMCI module is subjected to a transient condition, the adaptive control law ensures asymptotical stability and convergence. Now, it is obvious from Fig. 4 that, at any given time, only two out of the three modules of the three-phase DMCI are operating under high-frequency condition while the third module generates a null voltage. This poses a difference in the synthesis of modular control of a three-phase DMCI as compared to a single-phase DMCI. For instance, and as seen from the modes of operation shown in Fig. 4, for Module 1, for two modes of operation (Mode 3 and Mode 4), the load current only flows through Module 3 while in other modes (Mode 1 and Mode 2), the load current flows through Module 2 and Module 3. This dynamic change in Module-1's effective load needs to be addressed in the realization of the modular control of the three-phase DMCI along with the synthesis of a discontinuous-modulating signal, as shown in Fig. 5. Given this background on the subtle difference between the operations of a single- and three-phase DMCI, the same adaptive control algorithm can be adopted for the modular control of the DMCI since the control works effectively for time-varying operating condition(s).

A. Feedback-Gain ($k_x(t)$) Derivation and Tracking Stability

Let the Ćuk-converter module output model including the inverse transformation block as shown in Fig. 6 be outlined as follows [17]:

$$\dot{V}_{\text{out},x}(t) = \rho_{p,x} V_{\text{out},x}(t) + V_x(t) \tag{4}$$

where $\rho_{p,x}$ is the overall converter (including inverse transformation block and Ćuk DMCI module) parameter which defines the control input-to-output relation. It is difficult to obtain for practical applications because it changes when the input voltage and the load are changed. The control objective is to design a feedback control $V(t)$ such that all closed-loop-system signals are bounded and the module output $V_{\text{out},x}(t)$ tracks the output $V^r_{\text{out},x}(t)$ of a chosen reference model

$$\dot{V}^r_{\text{out},x}(t) = -\rho_{r,x} V^r_{\text{out},x}(t) + V_{\text{ref},x}(t), \quad t \geq 0 \tag{5}$$

with $V^r_{\text{out},x}(0)$, $\rho_{r,x} > 0$ for stability and performance, and $V_{\text{ref},x}(t)$ is a bounded external input which characterizes desired (reference) system response. If $\rho_{p,x}$ is known precisely, one can use the following feedback controller:

$$\begin{aligned} V_x(t) &= k^*_x V_{\text{out},x}(t) + V_{\text{ref},x}(t) \\ &= -(\rho_{p,x} + \rho_{r,x}) V_{\text{out},x}(t) + V_{\text{ref},x}(t) \end{aligned} \tag{6}$$

which yields the following:

$$\dot{V}_{\text{out},x}(t) = -\rho_{r,x} V_{\text{out},x}(t) + V_{\text{ref},x}(t). \tag{7}$$

Defining the tracking error as

$$e_x(t) = V_{\text{out},x}(t) - V^r_{\text{out},x}(t) \tag{8}$$

yields the following expression:

$$\dot{e}_x(t) = -\rho_{r,x} e_x(t) \tag{9}$$

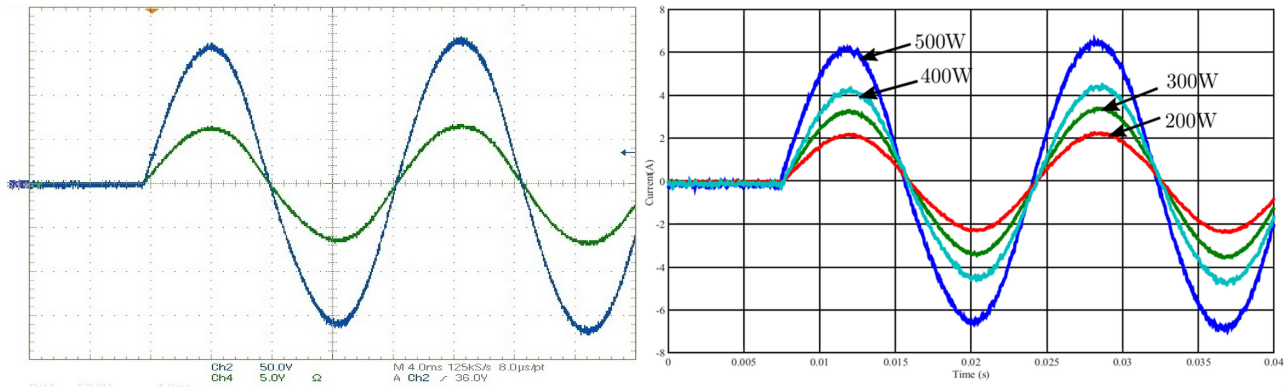

Fig. 8. (a) Experimental start-up output voltage (ch2) and output current (ch4) of the single-phase DMCI under rated-power resistive-load condition. (b) Experimental start-up response of the output current of the single-phase DMCI for varying load power indicating no inrush current.

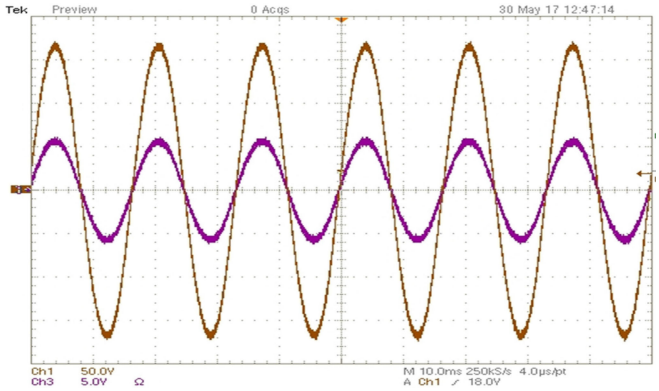

Fig. 9. Experimental steady-state output voltage (ch1) and output current (ch3) of the single-phase DMCI under resistive-load condition.

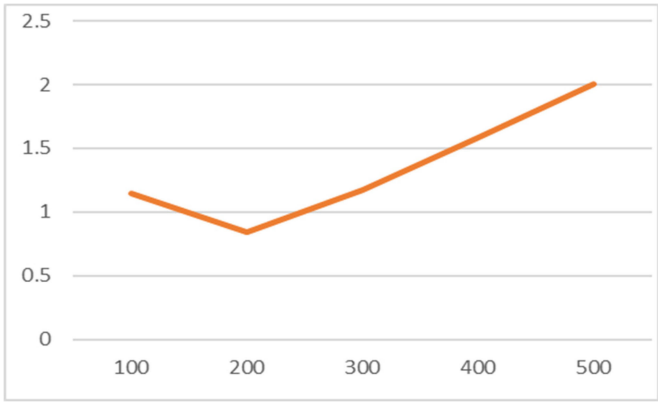

Fig. 11. Experimentally obtained THD in percentage (vertical axis) with varying load output power in watts (horizontal axis) for the single-phase DMCI.

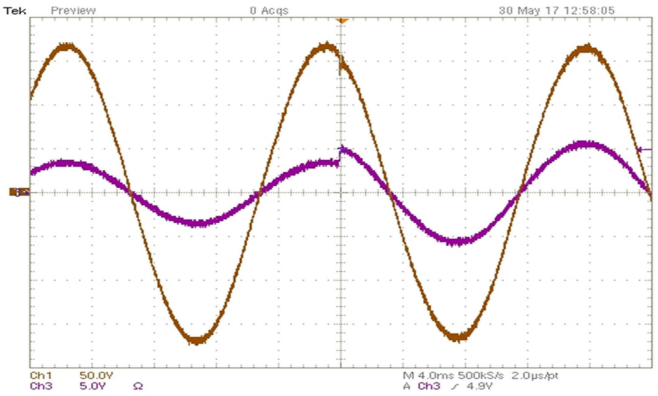

Fig. 10. Experimental output voltage (ch1) and output current (ch3) of the single-phase DMCI when the resistive-load power is changed from 300 to 500 W.

where $e_x(0) = V_{\text{out},x}(0) - V^r_{\text{out},x}(0)$. The solution to this equation is as follows:

$$e_x(t) = e^{-\rho_{r,x}t} e_x(0) \tag{10}$$

which has the desired property; that is, $e_x(t)$ is bounded and decreases exponentially.

For the DMCI module under consideration, one may not know the exact $\rho_{p,x}$; as such, one cannot implement the control law (6). So, one has to estimate feedback gain $k_x(t)$ to implement the adaptive controller that results in the following modified control law:

$$V_x(t) = k_x(t) V_{\text{out},x}(t) + V_{\text{ref},x}(t) \tag{11}$$

which yields the following:

$$\dot{V}_{\text{out},x}(t) = -\rho_{r,x} V_{\text{out},x}(t) + V_{\text{ref},x}(t) + \tilde{k}_x(t) V_{\text{out},x}(t) \tag{12}$$

where $\tilde{k}_x(t) = (k_x(t) - k^*)$. In terms of error, one obtains

$$e_x(t) = -\rho_{r,x} e_x(t) + \tilde{k}_x(t) V_{\text{out},x}(t). \tag{13}$$

Now, let us consider the Lyapunov function

$$V_x\left(e_x(t), \tilde{k}_x(t)\right) = e_x^2(t) + \frac{1}{\alpha_x}\tilde{k}_x^2(t) \tag{14}$$

where α_x represents the convergence factor, which determines how fast the output voltage of the DMCI module reaches steady state or how fast convergence is ensured. The time derivative of

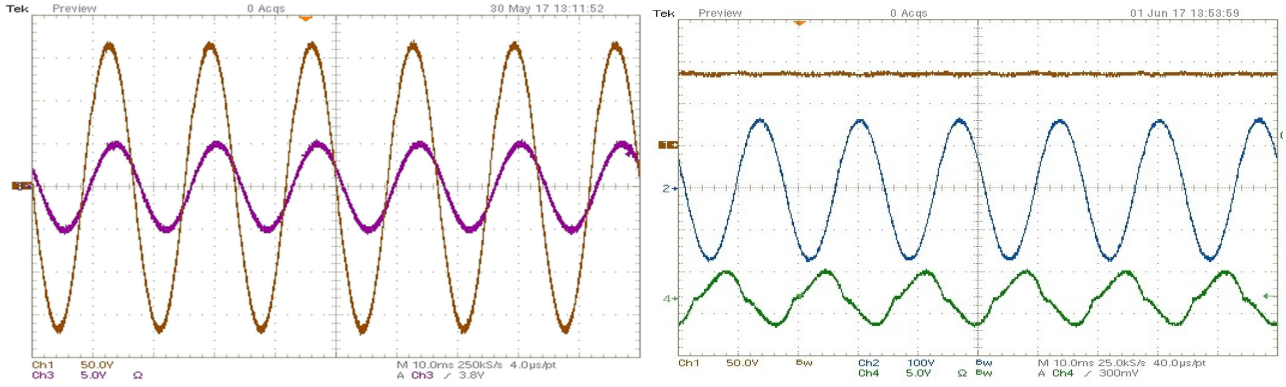

(a) (b)

Fig. 12. (a) Experimental steady-state output voltage (ch1) and output current (ch3) of the single-phase DMCI under reactive-load condition with a load resistance of 50 Ω and a load inductance of 32 mH. (b) Experimental steady-state output voltage (ch2) and output current (ch4) of the single-phase DMCI connected to a nonlinear-load (comprising a diode rectifier connected at the input to the DMCI output using a 27 mH inductance and at the output to a resistive-capacitive load) condition with a resistance of 50 Ω and a capacitance of 2.2 mF; the output dc voltage of the capacitor is shown in ch1.

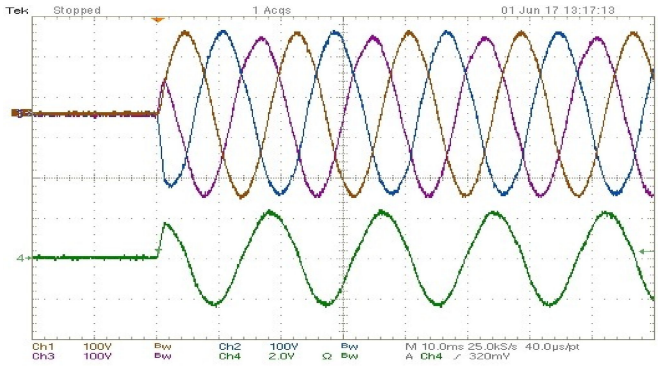

Fig. 13. Experimental start-up output line voltages (chs 1–3) and output current (ch4) of the three-phase DMCI under rated-power resistive-load condition.

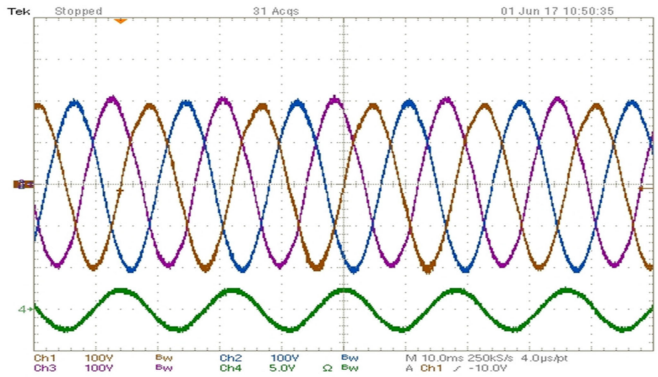

Fig. 14. Experimental steady-state output line voltages (chs 1–3) and output current (ch4) of the three-phase DMCI under resistive-load condition.

$V_x(e_x(t),\ \tilde{k}_x(t))$ yields the following expression:

$$\dot{V}_x\left(e_x\left(t\right),\ \tilde{k}_x\left(t\right)\right) = -2\rho_{r,x}e_x^2\left(t\right) + 2\tilde{k}_x\left(t\right)e_x\left(t\right)V_{\mathrm{out},x}\left(t\right) + \frac{2}{\alpha_x}\tilde{k}_x\left(t\right)\frac{d}{dt}\left(\tilde{k}_x\left(t\right)\right) \tag{15}$$

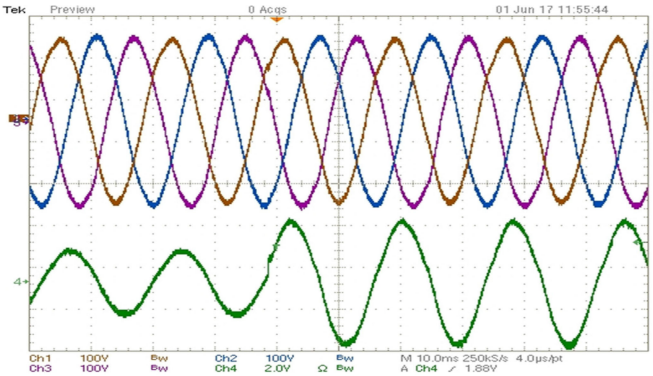

Fig. 15. Experimental output line voltages (chs 1–3) and output current (ch4) of the three-phase DMCI when the resistive-load power undergoes transience.

which needs to be less than zero to ensure Lyapunov stability (i.e., $\dot{V}_x(e_x(t),\ \tilde{k}_x(t)) < 0$). One way to ensure this requirement is to pose the following:

$$\frac{d}{dt}\left(\tilde{k}_x\left(t\right)\right) = \frac{d}{dt}\left(k_x\left(t\right) - k^*\right) = \frac{d}{dt}\left(k_x\left(t\right)\right) = -\alpha_x e_x\left(t\right)V_{\mathrm{out},x}\left(t\right) \tag{16}$$

which yields the following (shown earlier in this section):

$$k_x\left(t\right) = -\int_0^t \alpha_x e_x\left(\tau\right)V_{\mathrm{out},x}\left(\tau\right)d\tau + k_x\left(0\right).$$

This feedback-gain ($k_x(t)$) estimation yields robust tracking and stabilty.

B. Convergence of the Closed-Loop DMCI States

The nonlinearities of a DMCI-module equation arise due to the module hopping between various switching states, nonlinear adaptive controller, and the load if it is nonlinear. Using (16), which describes the first-order dynamical model of the adaptive nonlinear controller and assuming a quasi-static operation, the closed-loop model of the DMCI-module x is described by the

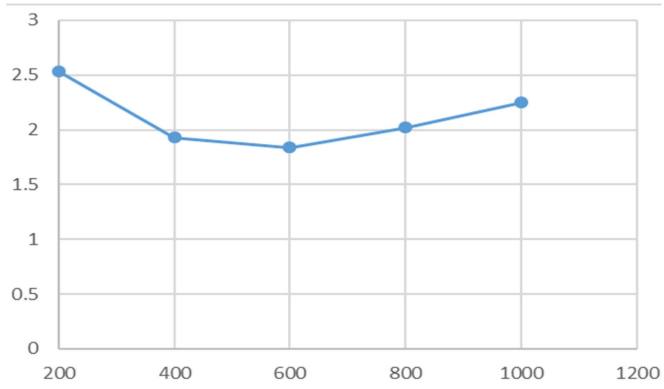

Fig. 16. Experimentally obtained THD in percentage (vertical axis) with varying output power in watts (horizontal axis) for the three-phase DMCI.

following weighted-hybrid-dynamical model [18]:

$$\dot{z}_x\left(t\right) = \dot{\sum}_{q=1}^{r} w_{qx}\left(z_x\left(t\right)\right)\left(A_{ql,x} z_x\left(t\right) + B_{ql,x}\right) \tag{17}$$

where l represent the switching states, $z_x(t)$ represents the states of the DMCI module and the adaptive controller, $w_{qx} : \Re \rightarrow \Re^{+}$ represents nonnegative scalar continuous weighting functions, $r = 2$ for the given model of the DMCI module, and the matrices $A_{ql,x}$ and $B_{ql,x}$ are described in Appendix A.

Now, we transform the hybrid model (17) to error coordinates using $y_x(t) = z_x^* - z_x(t)$, where $y_x(t)$ represents the states in the error coordinates and z_x^* represents the steady-state values of $z_x(t)$. The modified model takes the following form:

$$\dot{y}_x\left(t\right) = \sum_{q=1}^{r} w_{qx}\left(y_x\left(t\right)\right)\left(A_{ql,x} y_x\left(t\right) + \bar{B}_{ql,x}\right) \tag{18}$$

where $w_{1x} = 1$ and $w_{2x} = V_{\text{out},x}^2(t)$, and $\bar{B}_{qlx} = -(B_{ql,x} + A_{ql,x} z_x^*)$. To determine the criterion for convergence of the states of the module, a positive-definite-quadratic Lyapunov function, $V_{kq,x}(y_x(t)) > 0$ for the kth switching sequence (here $k = 1$ since a ramp carrier fixes the switching sequence), is selected which is given by the following [18] and [19]:

$$V_{kq,x}\left(y_x\left(t\right)\right) = \sum_{l=1}^{h} d_{kql,x} y_x(t)^T P_{kql,x} y_x\left(t\right) \tag{19}$$

where h is the number of switching states for the kth switching sequence, $P_{kql,x}$ represents a set of positive definite matrices (i.e., the minimum eigenvalue of each $P_{kql,x}$ is positive) $0 \leq d_{kql,x} = \frac{(\int_0^t -\alpha_x(V_{\text{ref},x} - V_{\text{out},x}(\tau))V_{\text{out},x}(\tau)d\tau) + V_{\text{ref},x}}{(\int_0^t -\alpha_x(V_{\text{ref},x} - V_{\text{out},x}(\tau))V_{\text{out},x}(\tau)d\tau) + V_{\text{ref},x} + 2*V_{\text{DC}}} \leq 1$ (which represents the proportion of the total time for the kth switching sequence that is spent in the hth switching state; it is obtained using (3) and (11) with relaxed initial condition for k_x, and $d_{kql,x} = \frac{V_x(t)}{V_x(t) + n*V_{\text{DC}}}$ with $n = 2$ following static linearization transformation in [8]) and $\sum_{l=1}^{h} d_{kql,x} = 1$. To show the reachability (i.e., convergence of the) states of a DMCI module to an orbit, one needs to ensure $\dot{V}_{kq,x}(y_x(t)) < 0$ for the qth subsystem, which, following [19] and [20], leads to the following linear-matrix inequality (LMI):

$$\sum_{l=1}^{h} d_{kql,x} \begin{bmatrix} y_x\left(t\right) \\ 1 \end{bmatrix}^T \begin{bmatrix} A_{ql,x}^T P_{kql,x} + P_{kql,x} A_{ql,x} & P_{kql,x}\bar{B}_{ql,x} \\ \bar{B}_{ql,x} P_{kql,x} & 0 \end{bmatrix} \times \begin{bmatrix} y_x\left(t\right) \\ 1 \end{bmatrix} < 0 \tag{20}$$

which is solved using a standard LMI tool in MATLAB [21]. If (20) yields a positive definite matrix $P_{kql,x}$ then that ensures the convergence of the closed-loop DMCI states to an orbit. Finally, following [22], to ensure that the converged orbit is a period-one orbit, a nonlinear map using the DMCI modular model is formed and Floquet theory is used to ensure that the Floquet multipliers or discrete eigenvalues of the map are within the unit circle.

IV. Experimental Results for the DMCI

Fig. 7 shows the image of the experimental multiphase DMCI. A TMS320F28335 digital signal processor was used to implement the control algorithm and to generate the PWM signals for all the DMCI modules. The code was so written such that the modularity of the implementation is ensured. The parameters of each module of the DMCI power stage are as follows for both single- and three-phase DMCI topological representations:

1) Input voltage: 35–80 V
2) Output voltage: 120/208 V (rms) for single/three phase
3) Switching frequency: 100 kHz
4) Input inductance: 50 μH
5) Output inductance: 100 μH
6) Transformer turns ratio (n): 2
7) Input blocking capacitance: 6 μF
8) Output blocking capacitance: 1.5 μF
9) Input capacitance: 1.5–3.3 mF (three/single phase)
10) Output capacitance: 4.4 μF
11) Load resistance: corresponding to 200–500 W (single/three phase) at rated voltage.

Further, experimental tests have also been carried out at rated DMCI output voltage for both single- and three-phase DMCI using an *RL* load (power factor of 0.76, $R = 32\ \Omega$, and $L = 32$ mH) and a nonlinear load: diode rectifier interfaced to the DMCI output via 27 mH inductor and rectifier followed by an *RC* load with $R = 50\ \Omega$ and $C = 2.2$ mF. The prototype DMCI board is used to capture both single- and three-phase experimental results. Initially, the experimental results of the single-phase DMCI are presented followed by the demonstration of the results for the three-phase DMCI. Further, detailed analytical results regarding the convergence of the closed-loop single- and three-phase DMCI module states using the adaptive controller are provided in Appendix B.

To implement the closed-loop adaptive control, it is necessary to determine what value of α_x should be used for optimal results. The selection of α_x is governed by stability consideration guided by Section III and the transient response and total harmonic distortion (THD). To do this, α_x was varied using a simple embedded auto-tuning DSP code for different operating conditions over a range of values provided by the stability criterion and is so chosen such that the output-voltage-THD is

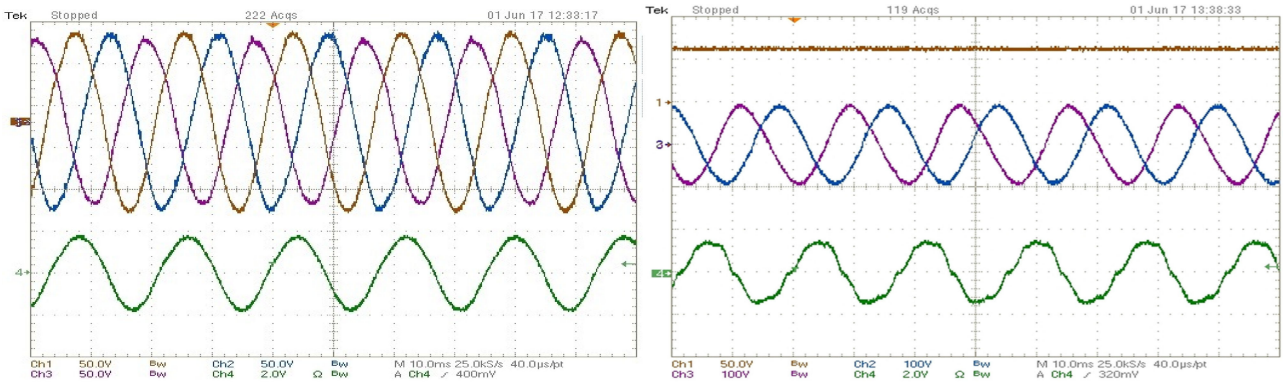

(a) (b)

Fig. 17. (a) Experimental steady-state output line voltages (chs 1–3) and output current (ch4) of the three-phase DMCI under reactive-load condition with a load resistance of 75 Ω and a load inductance of 32 mH. (b) Experimental steady-state output line voltages (chs 2 and 3) and output current (ch4) of the three-phase DMCI connected to a nonlinear-load (comprising diode rectifier connected at the input to the DMCI output using a 27 mH inductance and at the output to a resistive–capacitive load) condition with a resistance of 50 Ω and a capacitance of 2.2 mF; output dc voltage of the capacitor is shown in ch1.

at most two and the number of line cycles to reach the steady state is at most two for all operating conditions. Following this, $\alpha_x = 0.025$ is selected to carry out the experiments.

To begin with, the start-up waveform of single-phase DMCI under closed-loop condition at rated power and under resistive-load condition is shown in Fig. 8(a). It is noted that, for this result and subsequent ones, current expressed in terms of V/div represents A/div on a one-to-one basis (i.e., 1 V/div represent 1 A/div). The output voltage and output current reach the steady state promptly with a THD under 2% and acceptable tracking. Fig. 8 portrays the start-up response of the inverter. Fig. 9 shows the steady-state output voltage and output current. It is important to note that due to DMS, each module goes through transient after each line cycle.

Fig. 10 shows the dynamic response of the experimental output voltage and output current when the resistive-load power changes from 300 to 500 W. The figure clearly shows that the output voltage remains stable as the controller adapts to the changes in the load resistor and tracks the output voltage accurately.

Fig. 11 shows the THD of the single-phase DMCI's output voltage with varying resistive-load output power. The resistive output power in Fig. 11 is varied between 100 and 500 W at an input voltage of 40 V with the THD limited to close to 2%.

Finally, the responses of the single-phase DMCI are determined (as shown in Fig. 12) using reactive (*RL*) load with nominal resistance of 50 Ω and inductance of 32 mH and a nonlinear load (comprising a diode–rectifier interfaced to the DMCI output using 27 mH inductor at the front end and feeding a parallel combination of a capacitive filter of 2.2 mF and a resistor of magnitude 50 Ω at the output-end.

Next, the results of the three-phase DMCI are provided. Three Ćuk converter modules are controlled individually using a single DSP while keeping the modularity of the control algorithm. Similar to the single-phase DMCI implementation, α_x is varied for different operating conditions and then the best possible α_x is selected to ensure that the output THD and number of line cycles needed to reach the steady state are no higher than 3% and 2, respectively. For the three-phase DMCI, $\alpha_x = 0.025$ is found to satisfy the above-mentioned performance metrics. It is seen from Fig. 13 that the output line voltages and output current of the three-phase DMCI reaches the steady state rapidly from start-up condition and the transient is smooth without any spikes.

Fig. 14 shows the steady-state output line voltages and output current of the three-phase DMCI. It shows that there is limited distortion (with THD less than 2.6%) in the output voltage under steady-state condition distortion (with THD less than 2.6%) in the output voltage under steady-state condition.

Fig. 15 demonstrates experimentally the transient response of the output line voltages and output current when the load changes from 470 to 930 W. The figure clearly shows that the output voltage of the three-phase DMCI remains stable as the controller adapts to the changes in the load resistor and tracks the output voltage accurately.

Fig. 16 shows the THD output voltage of the three-phase DMCI with varying output power. The output power in Fig. 17 is varied between 100 and 500 W at an input voltage of 40 V. The THD is found to be below 2.6%.

Finally, the responses of the three-phase DMCI are determined (as shown in Fig. 17) using reactive (*RL*) load with nominal resistance of 50 Ω and inductance of 32 mH and a nonlinear load (comprising a diode-rectifier interfaced to the DMCI output using 27 mH inductor at the front end and feeding a parallel combination of a capacitive filter of 2.2 mF and a resistor of magnitude 50 Ω at the output-end.

V. Conclusion

A single- and a three-phase DMCI is implemented using a modular control, based on an adaptive control scheme, and needs a static-linearization transformation. Detailed outline on the controller tracking stability that leads to the desired adaptive gain and the convergence of the states of the closed-loop DMCI module operated using this nonlinear adaptive controller are provided. The stability proof uses a nonlinear approach and is a comprehensive and nontrivial one. The time-domain

experimental results for both the single- and three-phase DMCI for start-up, steady-state, and load-change conditions are found to be satisfactory. It is noted that the complex nonminimum phase and nonlinear dynamics of the DMCI along with tracking requirements in the presence of harmonics render the application of basic linear controllers relatively ineffective for such applications. Proportional-resonant compensators [7] are an option; however, tuning gains for individual harmonic components is a challenge and designing for stability is a nontrivial exercise. On a similar note, recursive controllers based on internal model principles [13] need careful nontrivial design with regard to delay control and may require an inner-loop controller. Nonlinear controllers such as sliding-mode control have been applied for Cuk-based converter topologies with promise. However, for isolated DMCI topology, sliding-mode control [23] is difficult to apply since constant frequency of operation is needed to ensure that the transformer core is not saturated. Moreover, sliding-mode controller will require plurality of sensing or partial sensing along with estimation. The latter will be needed for other sophisticated controllers such as those based on model prediction [24] or passivity [25]. Dynamic feedback linearization [26] may be a possibility as well; however, since DMCI is a higher order nonminimum phase system, the convergence of the zeroth-order dynamics, which is a nontrivial problem even for dc/dc Cuk converter, needs to be ensured for more complex time-varying DMCI.

For the modular control of the DMCI, the module reference involves multiple harmonics as well as dc components. By using the transformation based adaptive-gain tracking control, the desired reference is generated without frequency compartmentalization, which leads better dynamic response. This is also consistent with [13], with the exception that instead of wave-shaping harmonic compensation followed by a tracking controller, our proposition involves harmonic-mitigating transformation following a tracking controller. This also explains why compared to the results obtained earlier by our group using proportional-resonant-based harmonic-compensation control, the start-up results presented in this paper are found to be promising. For instance, the start-up times of the DMCIs reported using harmonic-compensation approach are in the order of a few line cycles while the corresponding results using the modular adaptive control scheme described in this paper exhibit limited delay under start-up condition. Even in the presence of load variations, the modular-control-based single- or three-phase DMCI is able to closely track the reference signal for the output voltage due to dynamic adaptation under stability bound. The closed-loop control system also yields low in-rush phase currents, which apart from tracking control (that enables slow build-up of output voltage from zero in small increments considering that the ratio of the line and switching frequencies is quite small and quasi-static condition holds), is also attributed to the low output capacitance of the DMCI that necessitate low charging current requirement, and precharging of the low-capacitance blocking capacitor to the input voltage. Finally, under periodic steady state, the THD results obtained for the single- and three-phase DMCIs using modular control are found to be satisfactorily low for varying output power.

APPENDIX A
MATRICES FOR (17) FOR DIFFERENT LOADS UNDER SINGLE- AND THREE-PHASE OPERATIONS

A. *Matrices for Single-Phase DMCI*

1) *R* Load

$$A_{11,x}=\begin{bmatrix} 0 & 0 & 0 & 0 & 0\\ 0 & 0 & \dfrac{1}{L_{px}}\left(2+\dfrac{C_{px}}{2\,C_{sx}}\right) & \dfrac{-1}{L_{sx}} & 0\\ 0 & \dfrac{-2}{C_{px}} & 0 & 0 & 0\\ 0 & \dfrac{1}{C_{ox}} & 0 & \dfrac{1}{RC_{0x}} & 0\\ 0 & 0 & 0 & -\alpha_x V_{\mathrm{ref},x} & 0 \end{bmatrix}$$

$$A_{12,x}=\begin{bmatrix} 0&0&0&0&0\\ 0&0&0&0&0\\ 0&0&0&0&0\\ 0&0&0&0&0\\ 0&0&0&0&0 \end{bmatrix}, B_{11,x}=\begin{bmatrix} \dfrac{V_{\mathrm{DC}}}{L_{px}}\\ 0\\ 0\\ 0\\ 0 \end{bmatrix},$$

$$B_{12,x}=\begin{bmatrix} 0\\ 0\\ 0\\ 0\\ \alpha_x V_{\mathrm{ref},x} \end{bmatrix}$$

$$A_{21,x}=\begin{bmatrix} 0 & 0 & \dfrac{1}{L_{px}}\left(-1-\dfrac{C_{px}}{4C_{sx}}\right) & 0 & 0\\ 0 & 0 & 0 & \dfrac{-1}{L_{sx}} & 0\\ \dfrac{1}{C_{px}} & 0 & 0 & 0 & 0\\ 0 & \dfrac{1}{C_{ox}} & 0 & \dfrac{1}{RC_{ox}} & 0\\ 0 & 0 & 0 & -\alpha_x V_{\mathrm{ref},x} & 0 \end{bmatrix},$$

$$B_{21,x}=\begin{bmatrix} \dfrac{V_{\mathrm{DC}}}{L_{px}}\\ 0\\ 0\\ 0\\ 0 \end{bmatrix} A_{22,x}=\begin{bmatrix} 0&0&0&0&0\\ 0&0&0&0&0\\ 0&0&0&0&0\\ 0&0&0&0&0\\ 0&0&0&0&0 \end{bmatrix},$$

$$B_{22,x}=\begin{bmatrix} 0\\ 0\\ 0\\ 0\\ \alpha_x V_{\mathrm{ref},x} \end{bmatrix}$$

where C_{px} (L_{px}) and C_{sx} (L_{sx}) are the primary- and secondary-side blocking capacitors (filter inductors) for module x that represent, respectively, C_a or C_c (L_a or L_c) and C_b or C_d (L_b or L_d). Similarly, C_{ox} represents either C_{o1} or C_{o2}.

2) *RL* Load

$$A_{11,x}=\begin{bmatrix}0 & 0 & 0 & 0 & 0 & 0\\ 0 & 0 & \frac{1}{L_{px}}\left(2+\frac{C_{px}}{2\,C_{sx}}\right) & \frac{-1}{L_{sx}} & 0 & 0\\ 0 & \frac{-2}{C_{px}} & 0 & 0 & 0 & 0\\ 0 & \frac{1}{C_{ox}} & 0 & 0 & \frac{-1}{C_{ox}} & 0\\ 0 & 0 & 0 & \frac{1}{L} & \frac{-R}{L} & 0\\ 0 & 0 & 0 & -\alpha_x V_{\mathrm{ref},x} & 0 & 0\end{bmatrix}$$

$$A_{12,x}=\begin{bmatrix}0&0&0&0&0&0\\0&0&0&0&0&0\\0&0&0&0&0&0\\0&0&0&0&0&0\\0&0&0&0&0&0\\0&0&0&0&0&0\end{bmatrix}, B_{11,x}=\begin{bmatrix}\frac{V_{\mathrm{DC}}}{L_{px}}\\0\\0\\0\\0\\0\end{bmatrix},$$

$$B_{12,x}=\begin{bmatrix}0\\0\\0\\0\\0\\\alpha_x V_{\mathrm{ref},x}\end{bmatrix}$$

$$A_{21,x}=\begin{bmatrix}0 & 0 & \frac{1}{L_{px}}\left(-1-\frac{C_{px}}{4C_{sx}}\right) & 0 & 0 & 0\\ 0 & 0 & 0 & \frac{-1}{L_{sx}} & 0 & 0\\ \frac{1}{C_{px}} & 0 & 0 & 0 & 0 & 0\\ 0 & \frac{1}{C_{ox}} & 0 & 0 & \frac{-1}{C_{ox}} & 0\\ 0 & 0 & 0 & \frac{1}{L} & \frac{-R}{L} & 0\\ 0 & 0 & 0 & -\alpha_x V_{\mathrm{ref},x} & 0 & 0\end{bmatrix}$$

$$A_{22,x}=\begin{bmatrix}0&0&0&0&0&0\\0&0&0&0&0&0\\0&0&0&0&0&0\\0&0&0&0&0&0\\0&0&0&0&0&0\\0&0&0&0&0&0\end{bmatrix}, B_{21,x}=\begin{bmatrix}\frac{V_{\mathrm{DC}}}{L_{px}}\\0\\0\\0\\0\\0\end{bmatrix},$$

$$B_{22,x}=\begin{bmatrix}0\\0\\0\\0\\0\\\alpha_x V_{\mathrm{ref},x}\end{bmatrix}.$$

3) Nonlinear Load

The periodically pulsating load current can be captured using a typical Fourier series of the following form, where $i_{ox1}^{1\mathrm{ph}}, i_{\mathrm{ox}2m}^{1\mathrm{ph}}$, and $i_{0x3m}^{1\mathrm{ph}}$ are determined using $i_{ox}^{1\mathrm{ph}}$

$$i_{ox}^{1\mathrm{ph}}=\frac{1}{2}i_{ox1}^{1\mathrm{ph}}+\sum_{n=1}^{\infty}\left\{i_{ox2m}^{1\mathrm{ph}}\cos(w_n t)+i_{ox3m}^{1\mathrm{ph}}\sin(w_m t)\right\}.$$

From simulation for a particular set of operating conditions the Fourier coefficients were calculated and used for the analysis. This leads to the following state-space parameters:

$$A_{11,x}=\begin{bmatrix}0 & 0 & 0 & 0 & 0\\ 0 & 0 & \frac{1}{L_{px}}\left(2+\frac{C_{px}}{2\,C_{sx}}\right) & \frac{-1}{L_{sx}} & 0\\ 0 & \frac{-2}{C_{px}} & 0 & 0 & 0\\ 0 & \frac{1}{C_{ox}} & 0 & 0 & 0\\ 0 & 0 & 0 & -\alpha_x V_{\mathrm{ref},x} & 0\end{bmatrix}$$

$$A_{12,x}=\begin{bmatrix}0&0&0&0&0\\0&0&0&0&0\\0&0&0&0&0\\0&0&0&0&0\\0&0&0&0&0\end{bmatrix}, B_{11,x}=\begin{bmatrix}\frac{V_{\mathrm{DC}}}{L_{px}}\\0\\0\\-i_{ox}^{1\mathrm{ph}}\\0\end{bmatrix},$$

$$B_{12,x}=\begin{bmatrix}0\\0\\0\\0\\\alpha_x V_{\mathrm{ref},x}\end{bmatrix}$$

$$A_{21,x}=\begin{bmatrix}0 & 0 & \frac{1}{L_{px}}\left(-1-\frac{C_{px}}{4C_{sx}}\right) & 0 & 0\\ 0 & 0 & 0 & \frac{-1}{L_{sx}} & 0\\ \frac{1}{C_{px}} & 0 & 0 & 0 & 0\\ 0 & \frac{1}{C_{ox}} & 0 & 0 & 0\\ 0 & 0 & 0 & -\alpha_x V_{\mathrm{ref},x} & 0\end{bmatrix}$$

$$A_{22,x}=\begin{bmatrix}0&0&0&0&0\\0&0&0&0&0\\0&0&0&0&0\\0&0&0&0&0\\0&0&0&0&0\end{bmatrix}, B_{21,x}=\begin{bmatrix}\frac{V_{\mathrm{DC}}}{L_{px}}\\0\\0\\-i_{\mathrm{ox}}^{1\mathrm{ph}}\\0\end{bmatrix}$$

$$B_{22,x}=\begin{bmatrix}0\\0\\0\\0\\\alpha_x V_{\mathrm{ref},x}\end{bmatrix}.$$

B. Matrices for Three-Phase DMCI

1) *R* Load unnum. eq. shown at the bottom of this page. where $d_x(t)$ is the duty ratio of the of the xth module while $L_2^{'}$ and L_2'' represent the secondary-side inductance of one of the remaining two modules, as shown in Fig. 1.

2) *RL* Load, unnum. eq. shown at the top of next page. where R and L represent the load resistance and inductance, $\beta_1 = \dfrac{L'_2\beta}{LR}$ $\beta_2 = \frac{L''_2}{L'_2 d_x(t)}$, and $\beta = L + L''_2 + \frac{LL''_2}{L'_2 d_x(t)}$.

3) Nonlinear Load

The periodically pulsating load current can be captured using a typical Fourier series of the following form, where $i_{ox1}^{3\text{ph}}$,$i_{ox2m}^{3\text{ph}}$,

$$A_{11,x} = \begin{bmatrix} 0 & 0 & 0 & 0 & 0 & 0 & 0 \\ 0 & 0 & \dfrac{1}{L_{px}}\left(2 + \dfrac{C_{px}}{2\,C_{sx}}\right) & \dfrac{-1}{L_{sx}} & 0 & 0 & 0 \\ 0 & \dfrac{-2}{C_{px}} & 0 & 0 & 0 & 0 & 0 \\ 0 & \dfrac{1}{C_{ox}} & 0 & 0 & \dfrac{-1}{C_{0x}} & \dfrac{-1}{C_{ox}} & 0 \\ 0 & 0 & 0 & \dfrac{1}{L''_2} & \dfrac{-2R}{L''_2} & \dfrac{-R}{L''_2} & 0 \\ 0 & 0 & 0 & \dfrac{1}{L'_2 d_x(t)} & \dfrac{-R}{L'_2 d_x(t)} & -\dfrac{1}{L'_2}\left(\dfrac{R}{d_x(t)} + R\right) & 0 \\ 0 & 0 & 0 & -\alpha_x V_{\text{ref},x} & 0 & 0 & 0 \end{bmatrix}$$

$$A_{12,x} = \begin{bmatrix} 0 & 0 & 0 & 0 & 0 & 0 & 0 \\ 0 & 0 & 0 & 0 & 0 & 0 & 0 \\ 0 & 0 & 0 & 0 & 0 & 0 & 0 \\ 0 & 0 & 0 & 0 & 0 & 0 & 0 \\ 0 & 0 & 0 & 0 & 0 & 0 & 0 \\ 0 & 0 & 0 & 0 & 0 & 0 & 0 \\ 0 & 0 & 0 & 0 & 0 & 0 & 0 \end{bmatrix}, B_{11,x} = \begin{bmatrix} \dfrac{V_{\text{DC}}}{L_{px}} \\ 0 \\ 0 \\ 0 \\ 0 \\ 0 \\ 0 \end{bmatrix}, B_{12,x} = \begin{bmatrix} 0 \\ 0 \\ 0 \\ 0 \\ 0 \\ 0 \\ \alpha_x V_{\text{ref},x} \end{bmatrix}$$

$$A_{21,x} = \begin{bmatrix} 0 & 0 & \dfrac{1}{L_{px}}\left(-1 - \dfrac{C_{px}}{4C_{sx}}\right) & 0 & 0 & 0 & 0 \\ 0 & 0 & 0 & \dfrac{-1}{L_{sx}} & 0 & 0 & 0 \\ \dfrac{1}{C_{px}} & 0 & 0 & 0 & 0 & 0 & 0 \\ 0 & \dfrac{1}{C_{ox}} & 0 & 0 & \dfrac{-1}{C_{ox}} & \dfrac{-1}{C_{ox}} & 0 \\ 0 & 0 & 0 & \dfrac{1}{L''_2} & \dfrac{-2R}{L''_2} & L''_2 & 0 \\ 0 & 0 & 0 & \dfrac{1}{L'_2 d_x(t)} & \dfrac{-R}{L'_2 d_x(t)} & -\dfrac{1}{L'_2}\left(\dfrac{R}{d_x(t)} + R\right) & 0 \\ 0 & 0 & 0 & -\alpha_x V_{\text{ref},x} & 0 & 0 & 0 \end{bmatrix}$$

$$A_{22,x} = \begin{bmatrix} 0 & 0 & 0 & 0 & 0 & 0 & 0 \\ 0 & 0 & 0 & 0 & 0 & 0 & 0 \\ 0 & 0 & 0 & 0 & 0 & 0 & 0 \\ 0 & 0 & 0 & 0 & 0 & 0 & 0 \\ 0 & 0 & 0 & 0 & 0 & 0 & 0 \\ 0 & 0 & 0 & 0 & 0 & 0 & 0 \\ 0 & 0 & 0 & 0 & 0 & 0 & 0 \end{bmatrix}, B_{21,x} = \begin{bmatrix} V_{\text{DC}} \\ 0 \\ 0 \\ 0 \\ 0 \\ 0 \\ 0 \end{bmatrix}, B_{22,x} = \begin{bmatrix} 0 \\ 0 \\ 0 \\ 0 \\ 0 \\ 0 \\ \alpha_x V_{\text{ref},x} \end{bmatrix}$$

$$A_{11,x}=\begin{bmatrix}0 & 0 & 0 & 0 & 0 & 0 & 0\\ 0 & 0 & \frac{1}{L_{px}}\left(2+\frac{C_{px}}{2\,C_{sx}}\right) & \frac{-1}{L_{sx}} & 0 & 0 & 0\\ 0 & \frac{-2}{C_{px}} & 0 & 0 & 0 & 0 & 0\\ 0 & \frac{1}{C_{\mathrm{ox}}} & 0 & 0 & \frac{-1}{C_{0x}} & \frac{-1}{C_{ox}} & 0\\ 0 & 0 & 0 & \frac{1}{\beta} & \frac{-2LR}{L'_2 d_x\,(t)\,\beta}-\frac{2R}{\beta} & \frac{LR}{L''_2}-\frac{R}{\beta} & 0\\ 0 & 0 & 0 & \frac{\beta_2}{\beta} & \frac{-\beta_2}{d_x\,(t)\,\beta_1}-\frac{2R\beta_2}{\beta}+\frac{R}{L'_2 d_x\,(t)} & \frac{\beta_2}{\beta_1}-\frac{R\beta_2}{\beta}-\frac{R}{L'_2 d_x\,(t)} & 0\\ 0 & 0 & 0 & -\alpha_x V_{\mathrm{ref},x} & 0 & 0 & 0\end{bmatrix}$$

$$A_{12,x}=\begin{bmatrix}0&0&0&0&0&0&0\\0&0&0&0&0&0&0\\0&0&0&0&0&0&0\\0&0&0&0&0&0&0\\0&0&0&0&0&0&0\\0&0&0&0&0&0&0\\0&0&0&0&0&0&0\end{bmatrix},B_{11,x}=\begin{bmatrix}\frac{V_{DC}}{L_{px}}\\0\\0\\0\\0\\0\\0\end{bmatrix},\ B_{12,x}=\begin{bmatrix}0\\0\\0\\0\\0\\0\\\alpha_x V_{ref,x}\end{bmatrix}$$

$$A_{21,x}=\begin{bmatrix}0 & 0 & \frac{1}{L_{px}}\left(-1-\frac{C_{px}}{4C_{sx}}\right) & 0 & 0 & 0 & 0\\ 0 & 0 & 0 & \frac{-1}{L_{sx}} & 0 & 0 & 0\\ \frac{1}{C_{px}} & 0 & 0 & 0 & 0 & 0 & 0\\ 0 & \frac{1}{C_{ox}} & 0 & 0 & \frac{-1}{C_{ox}} & \frac{-1}{C_{ox}} & 0\\ 0 & 0 & 0 & \frac{1}{\beta} & \frac{-2LR}{L'_2 d_x\,(t)\,\beta}-\frac{2R}{\beta} & \frac{LR}{L''_2}-\frac{R}{\beta} & 0\\ 0 & 0 & 0 & \frac{\beta_2}{\beta} & \frac{-\beta_2}{d_x\,(t)\,\beta_1}-\frac{2R\beta_2}{\beta}+\frac{R}{L'_2 d_x\,(t)} & \frac{\beta_2}{\beta_1}-\frac{R\beta_2}{\beta}-\frac{R}{L'_2 d_x\,(t)} & 0\\ 0 & 0 & 0 & -\alpha_x V_{\mathrm{ref},x} & 0 & 0 & 0\end{bmatrix}$$

$$A_{22,x}=\begin{bmatrix}0&0&0&0&0&0&0\\0&0&0&0&0&0&0\\0&0&0&0&0&0&0\\0&0&0&0&0&0&0\\0&0&0&0&0&0&0\\0&0&0&0&0&0&0\\0&0&0&0&0&0&0\end{bmatrix},\ B_{21,x}=\begin{bmatrix}\frac{V_{\mathrm{DC}}}{L_{px}}\\0\\0\\0\\0\\0\\0\end{bmatrix},\ B_{22,x}=\begin{bmatrix}0\\0\\0\\0\\0\\0\\\alpha_x V_{\mathrm{ref},x}\end{bmatrix}$$

and $i_{ox3m}^{3\mathrm{ph}}$ are determined using $i_{ox}^{3\mathrm{ph}}$:

$$i_{ox}^{3\mathrm{ph}}=\frac{1}{2}i_{ox1}^{3\mathrm{ph}}+\sum_{n=1}^{\infty}\left\{i_{ox2m}^{3\mathrm{ph}}\cos\left(w_m t\right)+i_{ox3m}^{3\mathrm{ph}}\sin\left(w_m t\right)\right\}.$$

From simulation for a particular set of operating conditions, the Fourier coefficients were calculated and used for the analysis. This leads to the following state-space parameters:

$$A_{11,x}=\begin{bmatrix}0 & 0 & 0 & 0 & 0\\ 0 & 0 & \frac{1}{L_{px}}\left(2+\frac{C_{px}}{2\,C_{sx}}\right) & \frac{-1}{L_{sx}} & 0\\ 0 & \frac{-2}{C_{px}} & 0 & 0 & 0\\ 0 & \frac{1}{C_{ox}} & 0 & 0 & 0\\ 0 & 0 & 0 & -\alpha_x V_{\mathrm{ref},x} & 0\end{bmatrix}$$

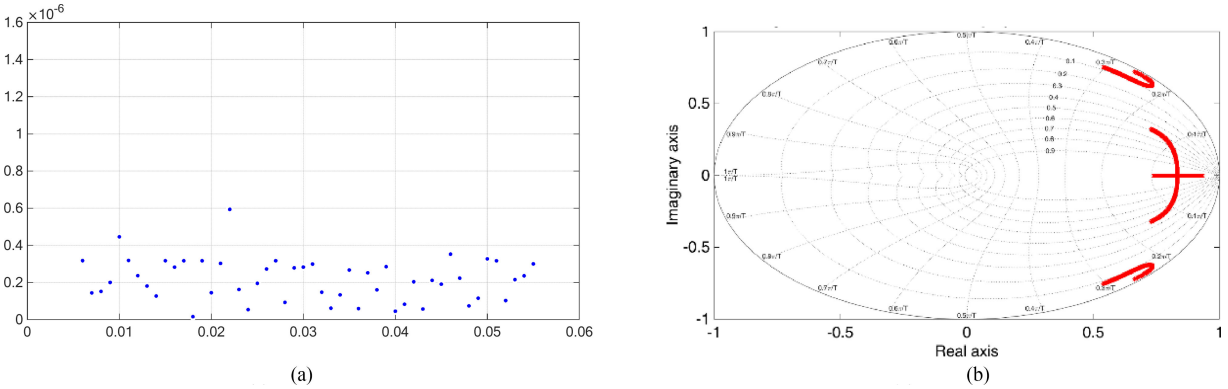

Fig. B1. (a) Minimum eigenvalue of P_{kql} (vertical axis) as a function α_x (horizontal axis), obtained using LMI, for the single-phase DMCI module operating with resistive load being positive proves orbital convergence of the module states. (b) Floquet multiplers (represented on imaginary and real axes) obtained using period-one map of the single-phase DMCI module model, being within the unit circle, establish that the period-one orbit is stable.

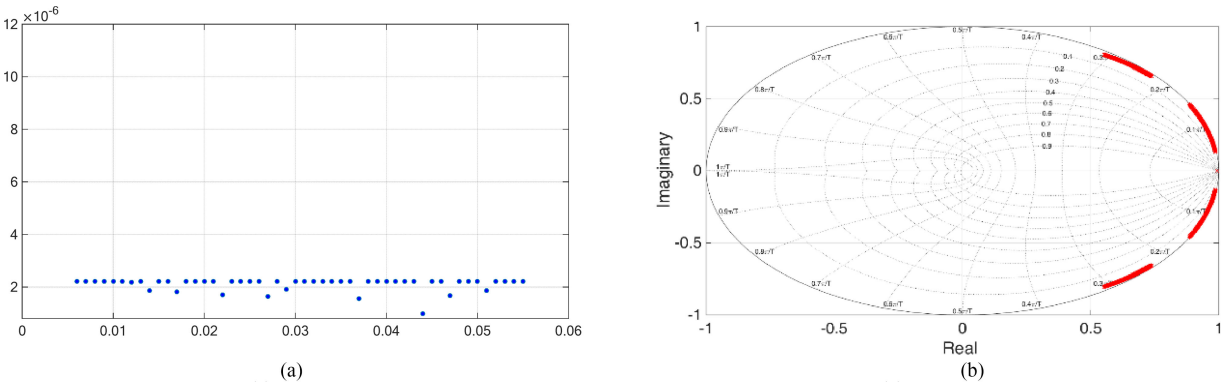

Fig. B2. (a) Minimum eigenvalue of P_{kql} (vertical axis) as a function α_x (horizontal axis), obtained using LMI, for the single-phase DMCI module operating with reactive (*RL*) load being positive proves orbital convergence of the module states. (b) Floquet multiplers (represented on imaginary and real axes) obtained using period-one map of the single-phase DMCI module model, being within the unit circle, establish that the period-one orbit is stable.

$$A_{12,x} = \begin{bmatrix} 0&0&0&0&0\\ 0&0&0&0&0\\ 0&0&0&0&0\\ 0&0&0&0&0\\ 0&0&0&0&0 \end{bmatrix}, B_{11,x} = \begin{bmatrix} \dfrac{V_{\rm DC}}{L_{px}}\\ 0\\ 0\\ -i_{ox}^{3ph}\\ 0 \end{bmatrix},$$

$$B_{12,x} = \begin{bmatrix} 0\\ 0\\ 0\\ 0\\ \alpha_x V_{{\rm ref},x} \end{bmatrix}$$

$$A_{21,x} = \begin{bmatrix} 0 & 0 & \dfrac{1}{L_{px}}\left(-1-\dfrac{C_{px}}{4C_{sx}}\right) & 0 & 0\\ 0 & 0 & 0 & \dfrac{-1}{L_{sx}} & 0\\ \dfrac{1}{C_{px}} & 0 & 0 & 0 & 0\\ 0 & \dfrac{1}{C_{ox}} & 0 & 0 & 0\\ 0 & 0 & 0 & -\alpha_x V_{{\rm ref},x} & 0 \end{bmatrix}$$

$$A_{22,x} = \begin{bmatrix} 0&0&0&0&0\\ 0&0&0&0&0\\ 0&0&0&0&0\\ 0&0&0&0&0\\ 0&0&0&0&0 \end{bmatrix}, B_{21,x} = \begin{bmatrix} \dfrac{V_{\rm DC}}{L_{px}}\\ 0\\ 0\\ -i_{ox}^{3\rm ph}\\ 0 \end{bmatrix},$$

$$B_{22,x} = \begin{bmatrix} 0\\ 0\\ 0\\ 0\\ \alpha_x V_{{\rm ref},x} \end{bmatrix}.$$

APPENDIX B
ANALYTICAL RESULTS OBTAINED FOLLOWING SECTION III-B REGARDING THE CONVERGENCE OF THE CLOSED-LOOP SINGLE- AND THREE-PHASE DMCI STATES USING THE ADAPTIVE CONTROLLER

See Figs. B1–B6.

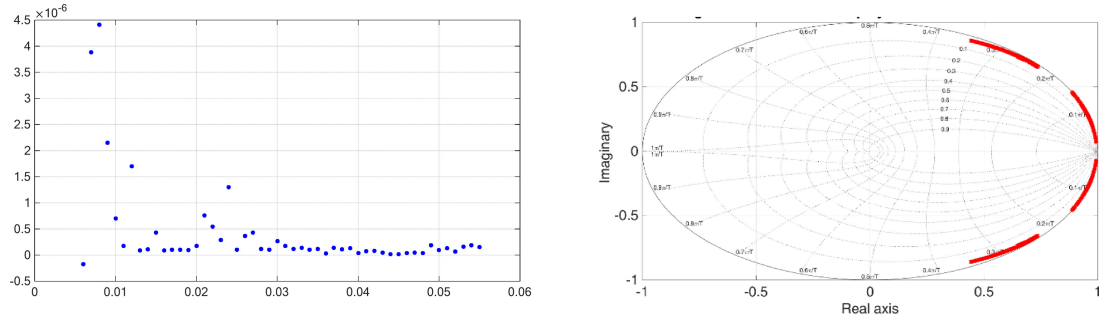

(a) (b)

Fig. B3. (a) Minimum eigenvalue of P_{kql} (vertical axis) as a function α_x (horizontal axis), obtained using LMI, for the single-phase DMCI module operating with nonlinear load being positive proves orbital convergence of the module states. (b) Floquet multipliers (represented on imaginary and real axes) obtained using period-one map of the single-phase DMCI module model, being within the unit circle, establish that the period-one orbit is stable.

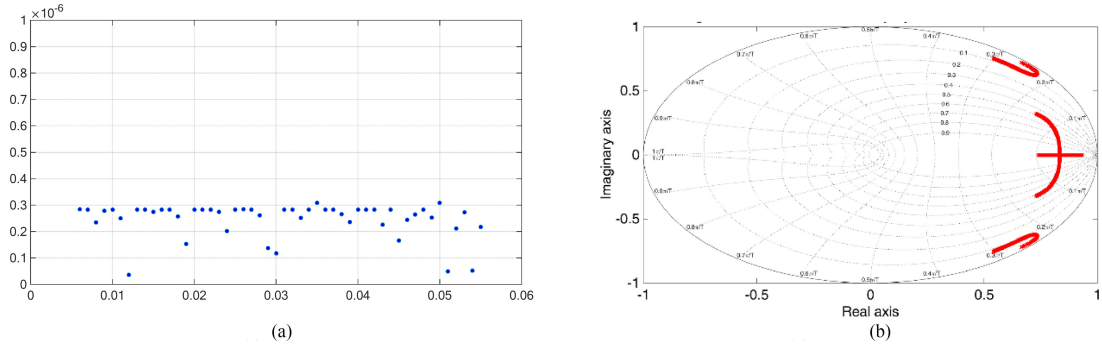

(a) (b)

Fig. B4. (a) Minimum eigenvalue of P_{kql} (vertical axis) as a function α_x (horizontal axis), obtained using LMI, for the three-phase DMCI module operating with resistive load being positive proves orbital convergence of the module states. (b) Floquet multipliers (represented on imaginary and real axes) obtained using period-one map of the three-phase DMCI module model, being within the unit circle, establish that the period-one orbit is stable.

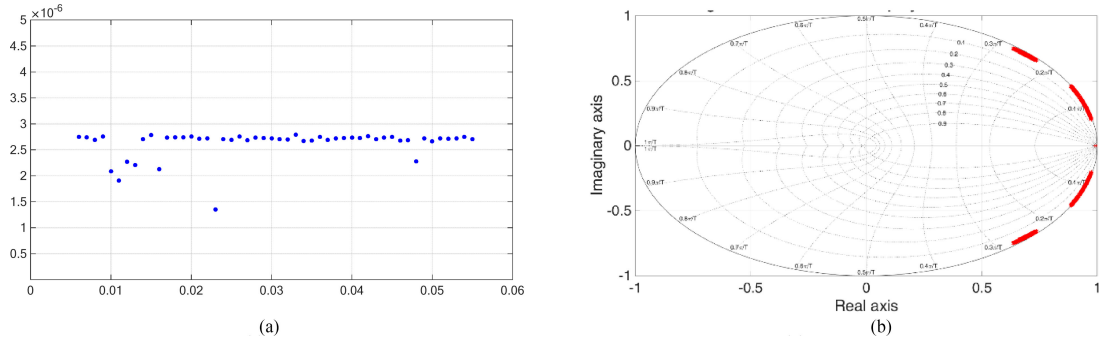

(a) (b)

Fig. B5. (a) Minimum eigenvalue of P_{kql} (vertical axis) as a function α_x (horizontal axis), obtained using LMI, for the three-phase DMCI module operating with reactive (*RL*) load being positive proves orbital convergence of the module states. (b) Floquet multipliers (represented on imaginary and real axes) obtained using period-one map of the three-phase DMCI module model, being within the unit circle, establish that the period-one orbit is stable.

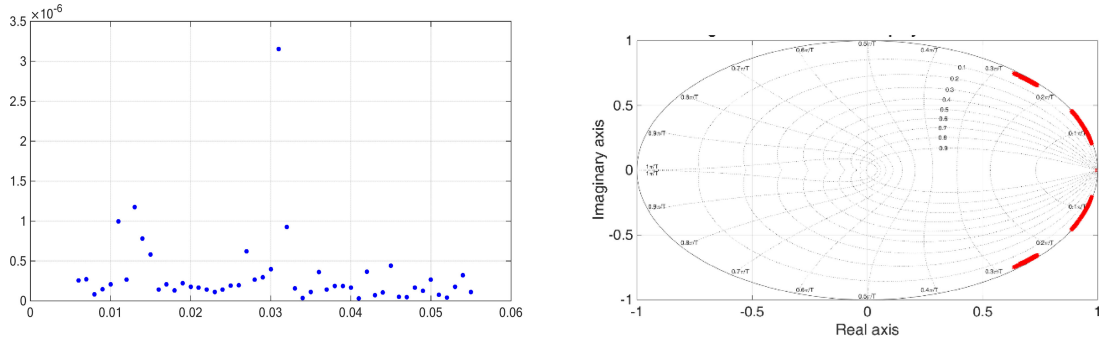

(a) (b)

Fig. B6. (a) Minimum eigenvalue of P_{kql} (vertical axis) as a function α_x (horizontal axis), obtained using LMI, for the three-phase DMCI module operating with nonlinear load being positive proves orbital convergence of the module states. (b) Floquet multipliers (represented on imaginary and real axes) obtained using period-one map of the three-phase DMCI module model, being within the unit circle, establish that the period-one orbit is stable.

REFERENCES

[1] S. K. Mazumder, J. W. Kolar, H. Akagi, and D. Xu, "Editorial: Special issue on high-frequency-link power-conversion," *IEEE Trans. Power Electron.*, vol. 29, no. 8, pp. 3849–3851, Aug. 2014.

[2] M. Amirabadi, J. Baek, H. A. Toliyat, and W. C. Alexander, "Soft-switching AC-link three-phase AC-AC buck–boost converter," *IEEE Trans. Ind. Electron.*, vol. 62, no. 1, pp. 3–14, Jan. 2015.

[3] Y. Liu, H. Abu-Rub, and B. Ge, "Front-end isolated quasi-Z-source DC–DC converter modules in series for high-power photovoltaic systems—Part I: Configuration, operation, and evaluation," *IEEE Trans. Ind. Electron.*, vol. 64, no. 1, pp. 347–358, Jan. 2017.

[4] B. Zhao, Q. Song, and W. Liu, "A practical solution of high-frequency-link bidirectional solid-state transformer based on advanced components in hybrid microgrid," *IEEE Trans. Ind. Electron.*, vol. 62, no. 7, pp. 4587–4597, Jul. 2015.

[5] S. Ćuk, "A new zero-ripple switching DC-to-DC converter and integrated magnetics," *IEEE Trans. Magn.*, vol. M-19, no. 2, pp. 57–75, Mar. 1983.

[6] J. M. A. Myrzik and M. Calais, "String and module integrated inverters for single-phase grid connected photovoltaic systems—A review," in *Proc. IEEE Power Technol. Conf.*, Bologna, Italy, Jun. 23–26, 2003, vol. 2, pp. 430–437.

[7] S. Mehrnami and S. K. Mazumder, "Discontinuous modulation scheme for a differential-mode Ćuk inverter," *IEEE Trans. Power Electron.*, vol. 30, no. 3, pp. 1242–1254, Mar. 2015.

[8] S. Mehrnami, S. K. Mazumder, and H. Soni, "Operation of a three-phase differential-mode Ćuk inverter using discontinuous modulation scheme," *IEEE Trans. Power Electron.*, vol. 31, no. 3, pp. 2654–2668, Mar. 2016.

[9] S. K. Mazumder and H. Soni, "Modular control of a differential-mode inverter," in *Proc. IEEE Energy Convers. Conf. Expo.*, 2015, pp. 3831–3837.

[10] R.-J. Wai, Y.-F. Lin, and Y.-K. Liu, "Design of adaptive fuzzy-neural-network control for single-stage boost inverter," *IEEE Trans. Power Electron.*, vol. 30, no. 12, pp. 7282–7298, Dec. 2015.

[11] R. O. Caceres and I. Barbi, "A boost DC–AC converter: Analysis, design, and experimentation," *IEEE Trans. Power Electron.*, vol. 14, no. 1, pp. 134–141, Jan. 1999.

[12] A. A. Khan, H. Cha, and H. F. Ahmed, "An improved single-phase direct PWM inverting buck-boost AC-AC converter," *IEEE Trans. Ind. Electron.*, vol. 63, no. 9, pp. 5384–5393, Sep. 2016.

[13] B. A. Francis and W. M. Wonham, "The internal model principle of control theory," *Automatica*, vol. 12, pp. 457–465, 1976.

[14] G. Tao, *Adaptive Control Design and Analysis*. Hoboken, NJ, USA: Wiley, 2003.

[15] M. Vidyasagar, *Nonlinear Systems Analysis*, 2nd ed. Englewood Cliffs, NJ, USA: Prentice-Hall, 1997.

[16] M. Krstic, I. Kanellakopoulos, and P. V. Kokotovic, *Nonlinear and Adaptive Control Design*. Hoboken, NJ, USA: Wiley, 1995.

[17] H. Soni, "Modular control of differential mode Ćuk inverter," M.S. thesis, Dept. Elect. Comput. Eng., Univ. Illinois, Chicago, IL, USA, Jul. 2015.

[18] S. Pettersson and B. Lennartson, "An LMI approach for stability analysis of nonlinear systems," in *Proc. Eur. Control Conf.*, 1997, pp. 1–6.

[19] S. K. Mazumder, R. Huang, and K. Acharya, "Rotor position feedback over an RF link for motor speed control," *IEEE Power Electron. Lett.*, vol. 25, no. 4, pp. 907–913, Apr. 2010.

[20] S. K. Mazumder and K. Acharya, "Multiple Lyapunov function based reaching criteria for orbital existence of switching power converters," *IEEE Trans. Power Electron.*, vol. 23, no. 3, pp. 1449–1471, May 2008.

[21] P. Gahinet, A. Nemirovskii, A. J. Laub, and M. Chilali, "The LMI control toolbox," in *Proc. IEEE Conf. Decision Control*, 1994, pp. 2038–2041.

[22] S. K. Mazumder, A. H. Nayfeh, and D. Boroyevich, "Theoretical and experimental investigation of the fast- and slow-scale instabilities of a DC/DC converter," *IEEE Trans. Power Electron.*, vol. 16, no. 2, pp. 201–216, Mar. 2001.

[23] J. Knight, S. Shirsavar, and W. Holderbaum, "An improved reliability Ćuk based solar inverter with sliding mode control," *IEEE Trans. Power Electron.*, vol. 21, no. 4, pp. 1107–1115, Jul. 2006.

[24] J. Neely, R. DeCarlo, and S. Pekarek, "Real-time model predictive control of the Ćuk converter," in *Proc. IEEE 12th Workshop Control Model. Power Electron.*, 2010, pp. 1–8.

[25] H. Rodrıguez, R. Ortega, and A. Astolfi, "Adaptive partial state feedback control of the DC-to-DC Cuk converter," in *Proc. IEEE Amer. Control Conf.*, Jun. 8–10, 2005, pp. 5121–5126.

[26] H. Sira-Ramirez and M. T. Prada-Rizzo, "Nonlinear feedback regulator design for the Cuk converter," *IEEE Trans. Automat. Control*, vol. 37, no. 8, pp. 1173–1180, Aug. 1992.

Harshit Soni received the bachelor's degree in electronics and communication engineering from the PES School of Engineering, Bengaluru, India, in 2012 and the M.S. degree in electrical and computer engineering from the University of Illinois at Chicago, Chicago, IL, USA, in 2015.

Since 2015, he has been with Tagore Technology as a Staff Engineer.

Sudip K. Mazumder (S'97–M'01–SM'03–F'16) received the Ph.D. degree in electrical and computer engineering from Virginia Tech, Blacksburg, VA, USA, in 2001.

Since 2001, he has been a Professor with the University of Illinois at Chicago (UIC), Chicago, IL, USA, and since 2008, has been the President of NextWatt LLC, Hoffman Estates, IL. He has more than 25 years of professional experience and has held R&D and design positions in leading industrial organizations, and has served as a Technical Consultant for several industries. He has authored or coauthored more than 200 refereed papers, delivered more than 85 keynote/plenary/invited presentations, and received and carried out about 50 sponsored research projects since joining UIC.

Ankit Gupta (S'11) received the B.E. degree in electrical engineering from the Delhi College of Engineering, Delhi, India, in 2011. Since 2013, he has been working toward the Ph.D. degree in electrical engineering at the University of Illinois at Chicago, Chicago, IL, USA.

From 2011 to 2013, he was with the Bharat Heavy Electrical Ltd., Haridwar, India.

Debanjan Chatterjee received the B.E. degree in electrical engineering from Jadavpur University, Kolkata, India, in 2015. He is currently working toward the Ph.D. degree in electrical and computer engineering at the University of Illinois at Chicago, Chicago, IL, USA.

Abhijit Kulkarni (S'05–M'16) received the Ph.D. degree in electrical engineering from the Department of Electrical Engineering, Indian Institute of Science, Bangalore, India, in 2016.

During July 2016–July 2017, he was a Postdoctoral Research Associate with the University of Illinois at Chicago, Chicago, IL, USA. He is a Technical Lead with the Honeywell Technology Solutions Lab. Pvt. Ltd., Bengaluru, India.